IEEE Photonics Journal
An IEEE Photonics Society Publication

Open Access

Dispersion Engineering in Single-Polarization Single-Mode Photonic Crystal Fibers for a Nearly Zero Flattened Profile

Volume 9, Number 5, October 2017

Dunke Lu
Xiaohang Li
Guohui Zeng
Jin Liu

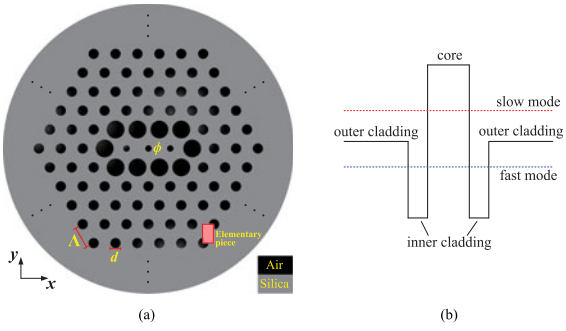

DOI: 10.1109/JPHOT.2017.2740951
1943-0655 © 2017 IEEE

IEEE photonics SOCIETY

IEEE

Dispersion Engineering in Single-Polarization Single-Mode Photonic Crystal Fibers for a Nearly Zero Flattened Profile

Dunke Lu, Xiaohang Li, Guohui Zeng, and Jin Liu

School of Electronic and Electrical Engineering, Shanghai University of Engineering Science, Shanghai 201620, China

DOI:10.1109/JPHOT.2017.2740951

Manuscript received March 22, 2017; revised August 11, 2017; accepted August 14, 2017. Date of publication August 21, 2017; date of current version August 29, 2017. Corresponding author: Dunke Lu (e-mail: ludunke@163.com).

Abstract: We propose a systematic solution to the problem on dispersion engineering in single-polarization single-mode (SPSM) photonic crystal fibers (PCFs) for a nearly zero flattened profile. Based on dispersion-approximating and -normalizing methods as well as a clever engineering strategy, we have succeeded in a design of SPSM PCF with nearly zero flattened dispersion $0.82 \pm 0.30\,\mathrm{ps/nm/km}$ over a broad band of $1.12 \sim 1.51\,\mu\mathrm{m}$. Moreover, such a fiber presents a very low confinement-loss level, which is less than 0.001 dB/km over the operation band.

Index Terms: Photonic crystal fibers, nearly zero flattened dispersion, single-polarization single mode, normalized disperson.

1. Introduction

Single-Polarization single-mode (SPSM) fibers support only one linearly polarized fundamental mode over a certain wavelength band, thus are free of the adverse crosstalk effect. Already these fibers have found important applications in optical systems, e.g., optical gyroscopes [1], [2] , fiber lasers with single-polarization output [3]–[5], Band-rejection filtering [6], polarization splitters [7], [8], and so on. In recent years, photonic crystal fibers (PCFs) as novel mediums are preferred to achieve broadband SPSM guidance [9]–[15], since their high index contrast between silica and air account for an appreciably high birefringence. Moreover, PCFs are generally composed of homogenous constituent (except for air), ensuring a more stable nature against temperature variation and stress imposition.

To date, controlling of chromatic dispersion for SPSM PCFs is still an ongoing challenge, imposing application restrictions in coherent communication systems as well as some nonlinear fields. It is well known that, flattening the dispersion in PCFs involves adjustments of structural parameters [16]–[25], including the lattice pitch and air-hole diameters. Nevertheless, varying these parameters is bound to shift the SPSM band, making troubles in dispersion flattening for such fibers. Although for the design in [15] we have observed a flattened dispersion profile by chance, but it is not broad as well as not close to zero. Since two airholes in the left and right side of the fiber core is not fixed for purpose of broadband SPSM operation, their variations will influence both the SPSM range

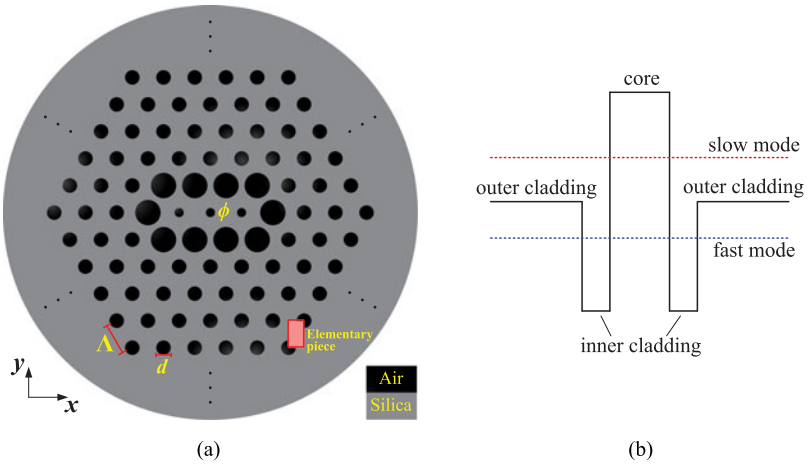

Fig. 1. (a) The cross-sectional schematic of the proposed SPSM PCF; (b) The equivalent refractive index profile of the fiber cross section.

and dispersion behaviour simultaneously, so it is hard to tailor the dispersion in such a design. Admittedly, there may exist some design parameter sets delivering a broad band of nearly-zero flattened profile, but it needs a lot of trial works to find them.

In this paper, we systematically describe a clever strategy integrating dispersion-approximating and -normalizing methods to design SPSM PCFs with nearly-zero flattened dispersion. The validation is done by using a full-vectorial finite element method, which has been proved highly accurate in mode calculations. Notice that the following design just considers all circular airholes arranged in a hexagonal lattice, thus it can be readily manufactured via the well-known stack and draw process.

2. Dispersion Engineering

The cross section of the proposed PCF architecture is schematically shown in Fig. 1(a). Circular airholes with diameters d, hexagonally latticed in silica background with pitch Λ, construct the typical photonic crystal cladding. In order to create a form birefringence, the fiber core is perturbed to resemble an oblong shape by introducing three contiguous airhole defects with diameters ϕ. It is worth saying that, assembling of airholes in the core can serve functions of, apart from tailoring the waveguide dispersion, heightening the birefringence so as to broaden the SPSM band. Additionally, ten airholes surrounding the core are enlarged with constant diameters of 0.9Λ to serve as a depressed inner cladding. The equivalent refractive index profile of such a configuration, as shown in Fig. 1(b), presents a W type accounting for the SPSM operation. When the fiber operates in the SPSM band, the effective index of outer cladding lies between that of the two orthogonally polarized fundamental modes, the one with higher effective index (slow mode, dashed red curve) can be preserved while the other one (fast mode, dashed blue curve) will leak out.

As for the outer cladding, its effective index is defined by the concept of fundamental space-filling mode (FSM) and can be calculated by imposing pairs of perfect electric/magnetic conditions on an elementary piece as depicted by a dashed area in Fig. 1(a). In the confining region, it is apparent that the dielectric interfaces predominately coincide with the x axis, thus the x-polarized fundamental mode $L\,P_{01}^{x}$ must have the highest effective index and should be preserved in case of SPSM operation. So, we stress here that, the following discussions on dispersion engineering only refer to the $L\,P_{01}^{x}$ mode.

In pursuing the SPSM design with nearly-zero flattened dispersion, we start with an assumption that, the size variation of outer-cladding airholes should takes very little effect on the dispersion profile at wavelengths far from the cutoff for a bound mode. This can be easily deduced from a fact that, the mode will only sees inner cladding as the effective fiber cladding when the mode

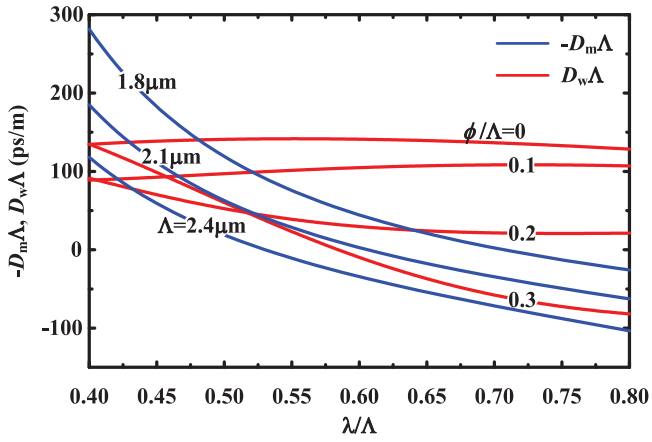

Fig. 2. The normalized waveguide dispersion (red curves) and negative normalized material dispersion (blue curves) as functions of the normalized wavelength λ/Λ for the LP_{01}^{x} mode.

field is tightly confined over the band of interest. Prior to the achievement of SPSM operation, outer-cladding airholes are first enlarged with $d = 0.9\Lambda$ to ensure all-band guidance for both the two orthogonally polarized fundamental modes. In such a case, adjustments of parameters ϕ and Λ can be made limitlessly to engineer a band of nearly-zero flattened dispersion for the LP_{01}^{x} mode. Then we will gradually decrease the size of outer-cladding airholes to generate and blue-shift cutoffs for the two fundamental modes, until the *y*-polarized fundamental mode LP_{01}^{y} vanishes over the dispersion-flattened band, leaving the only existent linearly polarized mode LP_{01}^{x}. If the dispersion-flattened property of this only existent mode can be verified to remain, we will succeed in the SPSM design with nearly-zero flattened dispersion.

Preliminarily, we use an approximating method to engineer a nearly-zero flattened dispersion profile for the PCF with $d = 0.9\Lambda$. In this method, the total dispersion D can be approximated as an algebraic sum of waveguide dispersion D_w and material dispersion D_m, i.e., $D \cong D_w + D_m$, which can be transformed to $D\Lambda \cong D_w\Lambda - (-D_m\Lambda)$, where $D_w\Lambda$ and $D_m\Lambda$ represents the normalized waveguide dispersion and normalized material dispersion, respectively. The transformed expression explicitly shows that, if the $D_w\Lambda$ and $-D_m\Lambda$ curves can be tailored as such that they nearly overlap, namely, $D_w\Lambda \cong (-D_m\Lambda)$ over a certain bandwidth, we will approximately meet the goal of nearly-zero flattened dispersion. In Fig. 2 we have shown the influence of parameter variations on the $D_w\Lambda$ and $-D_m\Lambda$ responses as functions of the normalized wavelength λ/Λ for the LP_{01}^{x} mode. Here, the waveguide dispersion is calculated assuming a constant silica index 1.45, while the material dispersion is calculated based on the Sellmeier equation. Notice that, in the normalized coordinate system, the lattice pitch Λ takes no effect on the normalized waveguide dispersion $D_w\Lambda$ (red curves), since it do not affect the mode effective index as a function of the normalized wavelength λ/Λ. Whereas, varying Λ can serve to alter $-D_m\Lambda$ (blue curves) when the material index is transformed to be a function of λ/Λ. It can be seen from Fig. 2 that, the Λ variation mainly causes the $-D_m\Lambda$ curves, which are concave in the band of interest, to move in verticality, but takes a slight effect on their slopes. On the other hand, varying airhole diameters ϕ/Λ in the core makes remarkable adjustments for the normalized waveguide dispersion $D_w\Lambda$. More importantly, a relative large ϕ/Λ value can produce a concave $D_w\Lambda$ curve in accord with $-D_m\Lambda$ curves, strongly contrasting a convex shape presented by a plain core ($\phi/\Lambda = 0$). Hence, we can fairly conclude that, it is precisely the existence of core airholes that make possible the overlap between the $D_w\Lambda$ and $-D_m\Lambda$ curves, inferring the potential achievement of a flattened total dispersion curve close to zero. In Fig. 3 we have shown a suitable parameter pair for the overlap attempt, that is, $\Lambda = 2.1\ \mu$m and $\phi/\Lambda = 0.27$. To exam these two approximate values, we have shown, in the inset of Fig. 3, the exact total dispersion D as a function of λ, for which the mode calculation directly take into account the wavelength dependence of the material index. Evidently, this curve presents a

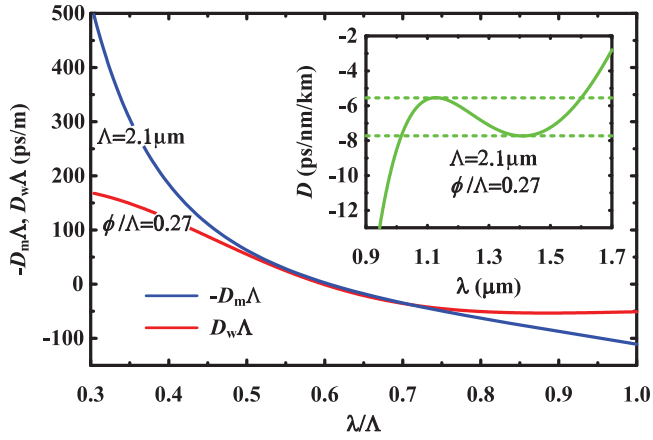

Fig. 3. The $D_w\Lambda$ response for $\phi/\Lambda = 0.2$ (red curve) and $-D_m\Lambda$ response for $\Lambda = 2.1\,\mu$m (blue curve). The inset shows the exact total dispersion D as a function of λ for the fiber with $\phi/\Lambda = 0.27$ and $\Lambda = 2.1\,\mu$m.

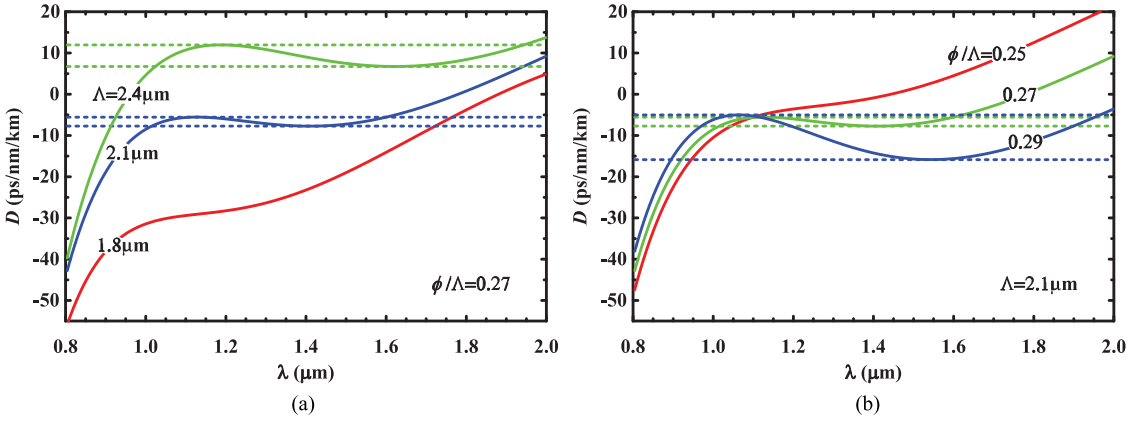

Fig. 4. (a) Total dispersion curves for $\phi/\Lambda = 0.27$ PCFs with different lattice pitches Λ; (b) total dispersion curves for $\Lambda = 2.1\,\mu$m PCFs with different defect diameters ϕ/Λ.

quasi-cubic profile with two extrema, implying the broadband flatness for the total dispersion. Moreover, the dispersion interval between these two extrema is centered at a low value of -6.6 ps/nm/km, indicating the potential of nearly-zero characteristic.

In order to improve the nearly-zero flattened behavior, we investigate the influences of parameters Λ and ϕ/Λ on the total dispersion. Fig. 4(a) shows total dispersion curves for $\phi/\Lambda = 0.27$ PCFs with different Λ values. It can be seen that, increasing the lattice pitch can move the flattened segment of the dispersion curve, which is delimited by its extrema, towards anomalous regions, accompanied by increments in both the dispersion interval and wavelength band of the flattened segment. Fig. 4(b) shows total dispersion curves for $\Lambda = 2.1\,\mu$m PCFs with different ϕ/Λ values. It can be seen that, increasing the defected diameter will extend both the dispersion interval and wavelength band of the flattened segment, which is mainly caused by a downwards movement of the lower extremum as well as a redshift of its corresponding wavelength. Conclusively, an increment in lattice pitch or defect diameter can broaden the flattened band, however, at the cost of flatness degradation. Besides, the wavelength band of flattened dispersion should not be broadened to exceed that of SPSM operation. On the other hand, too small values of lattice pitch or defect diameter, e.g. the red lines in Fig. 4, will transform the dispersion curve to be monotonous, hence completely destroying the flattened property. In view of the above observations, structural parameters are optimized to be $\Lambda = 2.2\,\mu$m and $\phi/\Lambda = 0.26$, corresponding to a flattened dispersion profile of

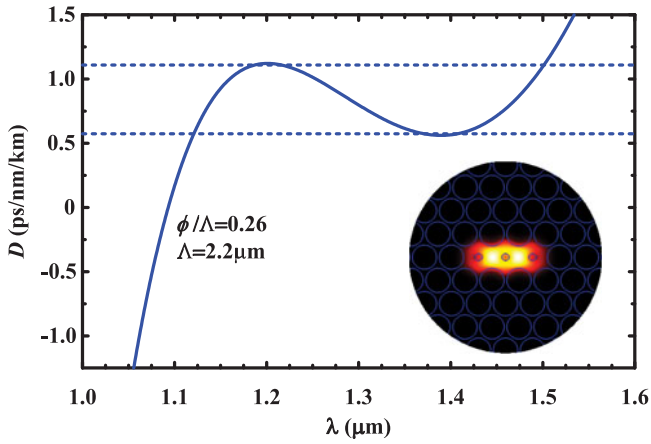

Fig. 5. The total dispersion for a PCF with $\Lambda = 2.2\,\mu$m and $\phi/\Lambda = 0.26$. The inset displays the mode intensity distribution at $\lambda = 1.31\,\mu$m.

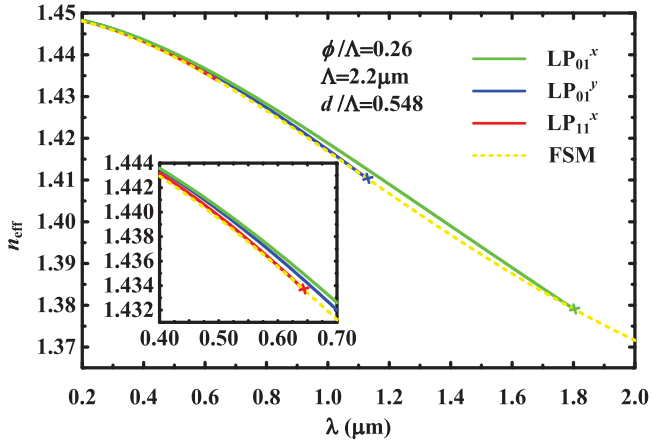

Fig. 6. Dispersive relations for a PCF with $d/\Lambda = 0.548$, including two fundamental modes LP_{01}^{x} and LP_{01}^{y}, the first higher-order mode LP_{11}^{x}, and the FSM. The inset is a blowup of the short-wavelength response.

0.84 ± 0.27 ps/nm/km within a wavelength band of $1.12 \sim 1.50\,\mu$m; this result is plotted in Fig. 5, which additionally comprises an inset displaying the mode intensity distribution at $\lambda = 1.31\,\mu$m.

3. SPSM Design

In what follows, we will decrease the size of outer-cladding airholes to generate differential cutoffs for the two fundamental modes, and hence to produce a wavelength band of SPSM operation. Notice the other two parameters, i.e. the lattice pitch and defect diameter is maintained to be $\Lambda = 2.2\,\mu$m and $\phi/\Lambda = 0.26$. In view of the abovementioned assumption, which implies that the dispersion profile can remain unchanged at short wavelengths far from the cutoff, and in order to reduce the confinement loss as much as possible for the only existent mode LP_{01}^{x}, the flattened band should be kept away as far as possible from the cutoff of this mode. It is therefore better to diminish the airhole diameter d/Λ to such a value that the LP_{01}^{y} mode is cut off just before the flattened band. In Fig. 6 we have shown dispersive relations for a PCF with such a desired value $d/\Lambda = 0.548$, including two fundamental modes and the first higher-order mode LP_{11}^{x}, as well as the FSM for predicting mode cutoffs. In regard of PCFs, a mode is cut off when its effective index falls through the FSM. Firstly, the LP_{11}^{x} mode is cut off at $\lambda = 0.64\,\mu$m, which can be clearly

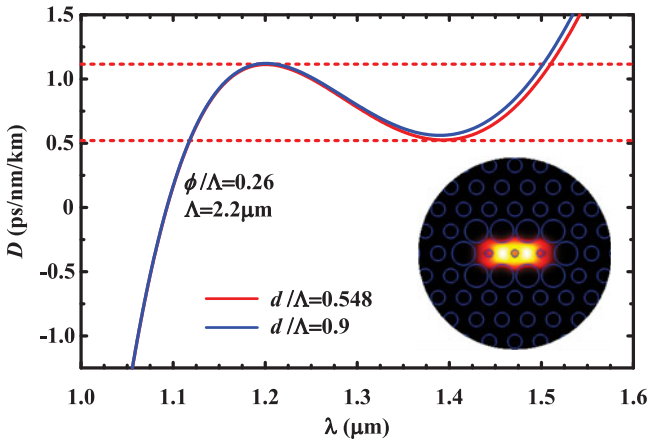

Fig. 7. Total dispersion curves for PCFs with $d/\Lambda = 0.548$ and $d/\Lambda = 0.9$, respectively, while other structural parameters share the same values $\Lambda = 2.2\,\mu$m and $\phi/\Lambda = 0.26$. The inset displays the mode intensity distribution for the PCF with $d/\Lambda = 0.548$ at $\lambda = 1.31\,\mu$m.

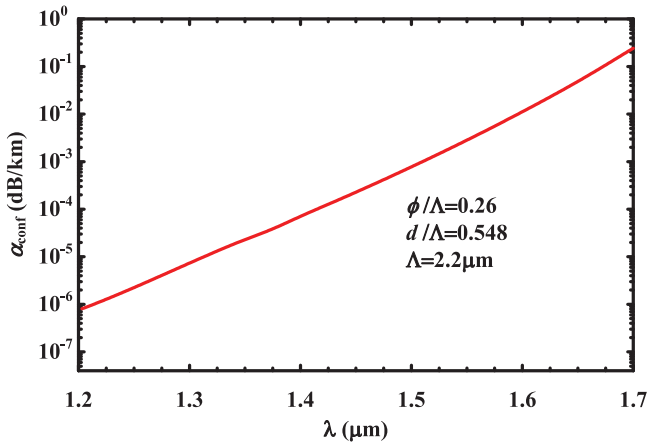

Fig. 8. The spectral confinement loss α_{conf} of the PCF with $\phi/\Lambda = 0.26$, $d/\Lambda = 0.548$ and $\Lambda = 2.2\,\mu$m.

observed in the blowup of short-wavelength responses. Subsequently, the $L\,P_{01}^{y}$ and $L\,P_{01}^{x}$ modes successively find their cutoffs at $\lambda = 1.12\,\mu$m and $\lambda = 1.80\,\mu$m, yielding a wide spectrum of 680 nm for SPSM operation, which completely covers the originally flattened band. This SPSM PCF should, as assumed, maintain the nearly-zero flattened property for the dispersion of the only existent mode $L\,P_{01}^{x}$. The verification is done by a comparison of dispersion curves between the SPSM PCF with $d/\Lambda = 0.548$ and the original one with $d/\Lambda = 0.9$, which is shown in Fig. 7. It can be confirmed from this figure that, the size variation of outer-cladding airholes indeed takes very little effect on the dispersion profile far from the cutoff. In particular at short wavelengths, the dispersion curve of the SPSM PCF almost overlaps with that of the original one, since both their mode fields are tightly confined in fiber cores, which share the same configuration. Whereas at long wavelengths, a small deviation can be observed between these two dispersion curves. This is because the SPSM PCF suffers a relatively stronger mode-field penetration into outer cladding over the long wavelengths, which are relatively closer to the cutoff. Since its outer cladding has been raised on account of decrements in airhole diameters, the mode effective index of this fiber is accordingly increased in comparison to that of the original one, thus yielding a slower decline in dispersive curve and hence a lower dispersion magnitude. Now we have succeed in the design of an SPSM PCF with a broad band of nearly zero flattened dispersion, that is 0.82 ± 0.30 ps/nm/km within $1.12 \sim 1.51\,\mu$m. For this fiber, the inset of Fig. 7 has additionally displayed the intensity distribution of the only existent

mode LP_{01}^{x} at $\lambda = 1.31\,\mu$m, which appears almost identical to that of the original one shown in Fig. 5. It is worth saying that, the dispersion behavior can be further improved, but it need more precise controls of structural parameters.

Finally, we calculate the confinement loss α_{conf} for the above designed dispersion-flattened SPSM PCF with a total number of eleven airhole rings, which is performed by imposing a perfect matched layer on the fiber boundary. Fig. 8 has shown the spectral loss for this fiber, which presents a very low level over the band of interest. Specially over the dispersion-flattened band, the confinement-loss level turns out to be lower than 0.001 dB/km. On the other hand, the presence of core airholes should give rise to scattering losses, whose accurate values can be measured through experiments.

4. Conclusion

In conclusion, we have described a systematic solution to the problem on dispersion engineering in W-type SPSM PCFs for a nearly zero flattened profile. Prior to the achievement of SPSM characteristic, outer-cladding airholes are first enlarged to share the same size as inner-cladding airholes. In such a case, the lattice pitch and core airholes can be limitlessly adjusted to engineer the dispersion property. Based on dispersion-approximating and -normalizing methods, a broad band of nearly zero flattened dispersion is preliminarily obtained in the fundamental mode with higher effective index. Then we decrease the size of outer-cladding airholes, which have been verified with very little effect on dispersion profile, to cut off other modes just before the nearly zero flattened band, leaving an only existent fundamental mode with dispersion $0.82 \pm 0.30\,$ps/nm/km over the $1.12 \sim 1.51\,\mu$m band. The confinement-loss level of such a fiber proves extremely low, even less than 0.001 dB/km over the operation band. Predictably, our design promise highly desired mediums in coherent communication systems as well as some nonlinear fields like supercontinuum generation with single-polarization output.

Acknowledgment

The authors wish to thank the anonymous reviewers for their valuable suggestions.

References

[1] H. Ma, Z. Chen, and Z. Jin, "Single-polarization coupler based on air-core photonic bandgap fibers and implications for resonant fiber optic gyro," *J. Lightw. Technol.*, vol. 32, no. 1, pp. 46–54, Jan. 2014.
[2] Y. Yan, H. Ma, and Z. Jin, "Reducing polarization-fluctuation induced drift in resonant fiber optic gyro by using single-polarization fiber," *Opt. Express*, vol. 23, no. 3, pp. 2002–2009, 2015.
[3] T. Schreiber *et al.*, "Stress-induced single-polarization single-transverse mode photonic crystal fiber with low nonlinearity," *Opt. Express*, vol. 13, no. 19, pp. 7621–7630, 2005.
[4] O. Schmidt *et al.*, "Single-polarization ultra-large-mode-area Yb-doped photonic crystal fiber," *Opt. Express*, vol. 16, no. 6, pp. 3918–3923, 2008.
[5] R. Goto, R. J. Williams, N. Jovanovic, G. D. Marshall, M. J. Withford, and S. D. Jackson, "Linearly polarized fiber laser using a point-by-point Bragg grating in a single-polarization photonic bandgap fiber," *Opt. Lett.*, vol. 36, no. 10, pp. 1872–1874, 2011.
[6] D.-R. Song, K. J. Lee, and B. Y. Kim, "Band-rejection filtering based on lossy torsional acousto-optic coupling in a single polarization fiber," *Opt. Express*, vol. 22, no. 20, pp. 24034–24043, 2014.
[7] Z. Zhang, Y. Tsuji, and M. Eguchi, "Design of polarization splitter with single-polarized elliptical-hole core circular-hole holey fibers," *IEEE Photon. Technol. Lett.*, vol. 26, no. 6, pp. 541–543, Mar. 2014.
[8] Z. Zhong, Z. Zhang, Y. Tsuji, and M. Eguchi, "Study on crosstalk-free polarization splitter based on square lattice single-polarization photonic crystal fibers," *IEEE J. Quantum Electron.*, vol. 52, no. 5, May 2016, Art. no. 7000107.
[9] M. Eguchi and Y. Tsuji, "Single-mode single-polarization holey fiber using anisotropic fundamental space-filling mode," *Opt. Lett.*, vol. 32, no. 15, pp. 2112–2114, 2007.
[10] M.-Y. Chen and Y.-K. Zhang, "Improved design of polarization-maintaining photonic crystal fibers," *Opt. Lett.*, vol. 33, no. 21, pp. 2542–2544, 2008.
[11] L. Wang, S. Lou, W. Chen, and H. Li, "Design of a single-polarization single-mode photonic crystal fiber with a near-gaussian mode field and wide bandwidth," *Appl. Opt.*, vol. 49, no. 32, pp. 6196–6200, 2010.
[12] P. Geng *et al.*, "Design of broadband single-polarization single-mode photonic crystal fiber based on index-matching coupling," *IEEE Photon. Technol. Lett.*, vol. 6, no. 24, pp. 452–454, Mar. 2012.
[13] D. Lu, X. Zhang, M. Chang, G. Wang, L. Pan, and S. Zhuang, "Endlessly single-polarization single-mode holey fibers with low confinement loss," *Opt. Lett.*, vol. 38, no. 15, pp. 2915–2918, 2013.

[14] X. Wang, S. Li, Q. Liu, G. Wang, and Y. Zhao, "Design of a single-polarization single-mode photonic crystal fiber filter based on surface plasmon resonance," in *Plasmonics*. New York, NY, USA: Springer, 2016, pp. 1–6.
[15] D. Lu and J. Liu, "Broadband single-polarization single-mode operation in photonic crystal fibers with hexagonally latticed circular airholes," *J. Lightw. Technol.*, vol. 34, no. 10, pp. 2452–2458, May 2016.
[16] N. Florous, K. Saitoh, and M. Koshiba, "The role of artificial defects for engineering large effective mode area, flat chromatic dispersion, and low leakage losses in photonic crystal fibers: Towards high speed reconfigurable transmission platforms," *Opt. Express*, vol. 14, no. 2, pp. 901–913, 2006.
[17] K. Saitoh, N. J. Florous, and M. Koshiba, "Theoretical realization of holey fiber with flat chromatic dispersion and large mode area: An intriguing defected approach," *Opt. Lett.*, vol. 31, no. 1, pp. 26–28, 2006.
[18] S. A. Razzak and Y. Namihira, "Proposal for highly nonlinear dispersion-flattened octagonal photonic crystal fibers," *IEEE Photon. Technol. Lett.*, vol. 20, no. 4, pp. 249–251, Feb. 2008.
[19] H. Ademgil and S. Haxha, "Highly birefringent photonic crystal fibers with ultralow chromatic dispersion and low confinement losses," *J. Lightw. Technol.*, vol. 26, no. 4, pp. 441–448, Feb. 2008.
[20] S. Kim, C.-S. Kee, and C. G. Lee, "Modified rectangular lattice photonic crystal fibers with high birefringence and negative dispersion," *Opt. Express*, vol. 17, no. 10, pp. 7952–7957, 2009.
[21] F. Shi, Y. Wu, M. Li, Y. Zhao, and L. Zhao, "Highly birefringent two-mode photonic crystal fibers with near-zero flattened dispersion," *IEEE Photon. J.*, vol. 3, no. 6, pp. 1181–1188, Dec. 2011.
[22] M. A. Islam and M. S. Alam, "Design optimization of equiangular spiral photonic crystal fiber for large negative flat dispersion and high birefringence," *J. Lightw. Technol.*, vol. 30, no. 22, pp. 3545–3551, Nov. 2012.
[23] S. E. Kim, B. H. Kim, C. G. Lee, S. Lee, K. Oh, and C.-S. Kee, "Elliptical defected core photonic crystal fiber with high birefringence and negative flattened dispersion," *Opt. Express*, vol. 20, no. 2, pp. 1385–1391, 2012.
[24] I. Abdelaziz, F. AbdelMalek, S. Haxha, H. Ademgil, and H. Bouchriha, "Photonic crystal fiber with an ultrahigh birefringence and flattened dispersion by using genetic algorithms," *J. Lightw. Technol.*, vol. 31, no. 2, pp. 343–348, Jan. 2013.
[25] T. Martynkien, D. Pysz, R. Stepień, and R. Buczyński, "All-solid microstructured fiber with flat normal chromatic dispersion," *Opt. Lett.*, vol. 39, no. 8, pp. 2342–2345, 2014.